

## Cobalt oxide nanoparticles for biological applications: Synthesis and physicochemical characteristics for different natural fuels

C. Arun Paul<sup>a</sup>, E. Ranjith Kumar<sup>b,\*</sup>, A.F. Abd El-Rehim<sup>c</sup>, G. Yang<sup>d</sup>

<sup>a</sup> Department of Science and Humanities, Sri Krishna College of Engineering and Technology, Coimbatore, 641 008, Tamilnadu, India

<sup>b</sup> Department of Physics, KPR Institute of Engineering and Technology, Coimbatore, 41 407, Tamilnadu, India

<sup>c</sup> Physics Department, Faculty of Science, King Khalid University, P.O. Box 9004, Abha, 61413, Saudi Arabia

<sup>d</sup> State Key Laboratory of Precision Blasting, Jianghan University, Wuhan, 430056, China

### ARTICLE INFO

Handling Editor: Dr P. Vincenzini

**Keywords:**

Co<sub>3</sub>O<sub>4</sub> NPs  
Natural fuels  
Thermal properties  
Biomedical applications

### ABSTRACT

Cobalt oxide (Co<sub>3</sub>O<sub>4</sub>) nanoparticles were synthesized via a simple combustion process employing natural fuels, and their structural, morphological, thermal, and antibacterial properties were studied. According to XRD measurements, each specimen has a cubic crystalline structure. Co<sub>3</sub>O<sub>4</sub> nanoparticles prepared from natural macromolecules such as cow urine, honey, wine, and tea extract had respective crystallite diameters of 22.9, 31.3, 30.4, and 31.2 nm. According to FESEM and EDAX analyses, the products have stoichiometric shapes such as rice grains, mushrooms, and cluster cavities, and EDX confirmed the presence of the Co and O elements. The FTIR image revealed the presence of various phytochemicals on the surface, and the bands at 400 and 630 cm<sup>-1</sup> denoted the distinctive Co–O linkages. The diameters of crystallites and TEM particles are comparable. The thermal properties of Co<sub>3</sub>O<sub>4</sub> nanoparticles synthesized with diverse natural fuels are characterized by substantial weight losses. The particle's colloidal stability has been investigated. It confirms that the use of natural resources influences particle stability. Antibacterial and antifungal activity of green synthesized Co<sub>3</sub>O<sub>4</sub> nanoparticles was evaluated against two distinct bacteria (Gram-positive) *Staphylococcus aureus* and (Gram-negative) *Pseudomonas aeruginosa*, as well as two fungi, *Candida albicans* and *Aspergillus niger*. It has been discovered that synthetic Co<sub>3</sub>O<sub>4</sub> nanoparticles inhibit microbial and fungal proliferation effectively.

### 1. Introduction

The production of metal oxide nanoparticles (NPs) utilizing diverse ways has been hot issue of recent research. The primary focus is on energy applications, for instance, energy production and storage [1–8], sensor applications such as gas sensors, pharmaceuticals, and electrochemical medications, and medical applications such as antibacterial and anti-cancer treatment. Several metal oxide nanoparticles, including copper, titanium, zinc, alginate, gold, magnesium, and silver, are used as tunable semiconductors [9–13]. The most stable cobalt oxide is applied widely to lithium-ion batteries [14], gas sensors [15], magnetic storage [16], supercapacitors [17], and anti-microbial [18]. Recently, a hybrid technique of decreasing the use of inorganic solvents and natural reducing agents has been developed to reduce environmental pollution while achieving optimal repeatability in the synthesis process. After successfully synthesizing Co<sub>3</sub>O<sub>4</sub> nanoparticles with bentonite, Abdel Salam et al. [19] looked into their potential as eco-friendly, low-cost

adsorbents and photocatalysts for the removal of Cr(VI) ions and the malachite green dye (MG.D). Khalid, N. et al. [20] used green chilli and sunflower seed extracts to produce Co<sub>3</sub>O<sub>4</sub> nanoparticles. The recombination rate was shown to be the lowest in Co<sub>3</sub>O<sub>4</sub> nanoparticles made from sunflower extracts, as measured by photoluminescence (PL) experiments. Co-SF, when exposed to UV–Vis light, has shown the highest photodegradation activity (90%) among Co-P, Co-GC, and Co-SF photocatalysts against the water pollutant methylene blue (MB). In addition, the catalytic stability of this sample presented excellent, coming in at roughly 80.7%. Akshatha, S. et al. [21] used a straightforward microwave-aided green chemical approach to create synthetic carbon spheres covered with cobalt oxide nanoparticles that can interact with visible light. Cobalt–carbon spheres with a 6% mass ratio showed the highest photocatalytic activity. Batool, S. et al. [22] proposed an environmentally friendly method to create an incubating ZnO–Fe<sub>2</sub>O<sub>3</sub>–Co<sub>3</sub>O<sub>4</sub> nanocomposite from Cordia myxa. The peak on 508 and 387, corresponding to an I-NC energy bandgap of 2.2 eV, was confirmed by UV–Vis

\* Corresponding author.

E-mail address: [ranjueaswar@gmail.com](mailto:ranjueaswar@gmail.com) (E. Ranjith Kumar).

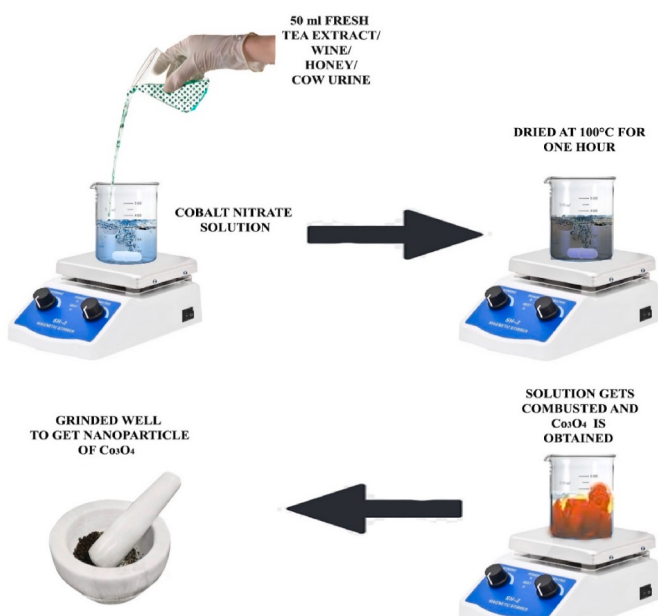


**Fig. 1.** Graphical representation of the green synthesis of  $\text{Co}_3\text{O}_4$  NPs using Tea extract, wine, Honey, and Cow urine. (For interpretation of the references to colour in this figure legend, the reader is referred to the Web version of this article.)

spectroscopy. In addition to its potential use as a photocatalytic agent, they suggested that using *Cordia myxa* in incubation nanocomposite manufacturing could serve as a novel antibacterial agent capable of limiting bacterial proliferation and biofilm formation. To produce  $\text{Co}_3\text{O}_4$  nanoparticles, Poonguzhal, R.V. et al. [23] used an auto-combustion technique aided by freshly squeezed lemon juice. Researchers have looked into the potential of  $\text{Co}_3\text{O}_4$  nanoparticles as LPG-based sensors with versatile detection capabilities. The results demonstrate that the synthesized nanoparticles have the potential to serve as an effective sensing material for LPG,  $\text{CO}_2$ , and  $\text{NH}_3$ . Chen, Q.-Y. et al. [24] reported an green synthesis of  $\text{Co}_3\text{O}_4$  nanoparticles with cobalt nitrate

hexahydrate and bread fungus. Hydrogen and oxygen are found to evolve at a quicker rate with increasing temperature, with the atomic ratio of hydrogen to oxygen approaching 2:1. This study presents a straightforward strategy for producing eco-friendly, high-performance photocatalysts made from cobalt oxide at a reasonable cost. *Solanum tuberosum* leaf extract was employed as a starting point for the production of  $\text{Co}_3\text{O}_4$  NPs with different surface-to-volume ratios by Bekele, E.T. et al. [25]. The highly catalytic behaviour and the more uniform surface structure may be to blame for this. Increased reactive oxygen species (ROS) production is linked to the 16-fold increase in  $\text{Co}_3\text{O}_4$  (1:2) nano drug's antibacterial effectiveness against *S. aureus*.  $\text{Co}_3\text{O}_4$  nanoparticles were studied by C.M. Magdalane et al. [26] for photocatalytic destruction of hazardous wastes from the dye industry, among other potential uses. Biosynthetic synthesis, they said, significantly reduced toxicity of  $\text{Co}_3\text{O}_4$ .  $\text{Co}_3\text{O}_4$  NPs were prepared by A. Khalil et al. [27] through the precipitation of a cobalt sulphate solution at a basic pH. Using a self-association strategy supported by heat denaturation, they created an agar-aqueous  $\text{Co}_3\text{O}_4$  (AG-  $\text{Co}_3\text{O}_4$ ) nanocomposite. This research demonstrated the significant potential of the AG-  $\text{Co}_3\text{O}_4$  catalyst in treating wastewater for pollution. Bael gum (BG) and its carboxymethylated (CMBG) derivative were used in a simple microwave-assisted production of palladium nanoparticles (Pd NPs) as described by K. Seku et al. [28]. Carboxymethylated Pd NPs were discovered to be smaller (7 nm) than Bael gum-capped Pd NPs (10 nm). Arishta leaves (also called Neem leaves) extract is used to produce a new biosynthesis of  $\text{Co}_3\text{O}_4$  NPs by Anuradha, C. et al. [29]. Prabaharan, D et al. infer that the antimicrobial and antibacterial properties of neem  $\text{Co}_3\text{O}_4$  NPs result from the specifics of their synthesis, including pH, reaction temperature, reaction time, and extract clustering. These results demonstrate that leaf extract can function as a dynamic response medium in  $\text{Co}_3\text{O}_4$  NP production.  $\text{BiFeO}_3$  nanoparticles were used by Asih Indriyani et al. in their study utilizing ALE, an extract made from the leaves of *Abelmoschus esculentus* L. Alkaloids, which are secondary metabolite compounds, can be used in place of dangerous chemicals like  $\text{NH}_4\text{OH}$  and  $\text{NaOH}$  as hydrolyzing agents and saponins and flavonoids as capping agents while making  $\text{BiFeO}_3$  nanoparticles.  $\text{BiFeO}_3$  underwent several characterization methodologies analysis in order to examine the properties. As a result, the analysis of the morphology and particle size demonstrated that  $\text{BiFeO}_3$  has a spherical form and a particle size of around 9.74 nm. We looked at the photocatalytic activity of  $\text{BiFeO}_3$  nanoparticles for the breakdown of methylene blue (MB) when exposed to visible light. After 120 min of exposure,  $\text{BiFeO}_3$  showed a 94.04% MB degradation percentage. The narrow bandgap energy of  $\text{BiFeO}_3$ , which was determined to be 2.00 eV, may be responsible for the high photocatalytic activity [30]. Rizki Marcony Surya et al. claims that due to the negative effects of its accumulation on aquatic systems, malachite green (MG) plays a role in water contamination. With the aid of *Alstonia scholaris* leaves extract (ASLE), which acts as natural hydrolyzing and stabilising agents, we successfully create a high photoresponse  $\text{ZnO}/\text{SmMnO}_3$  heterojunction for the first time. Under the illumination of visible light, the heterojunction formation increases  $\text{ZnO}$ 's photocatalytic activity by up to 91.74%.  $\text{SmMnO}_3$  alteration results in more separation of photogenerated charges and lower rates of electron-hole recombination, which results in a high rate of photodegradation of MG, according to photoluminescence study. For MG degradation over  $\text{ZnO}/\text{SmMnO}_3$ , the TOC removal efficiency was found to be 53.09% with 3 mg of catalyst, which is greater than that over  $\text{ZnO}$ . The pseudo-first-order kinetics model for the photocatalytic reaction had excellent stability across four cycles without structural change. According to the radical trapping experiment, the main species involved in the MG photodegradation reaction was  $\text{h}^+$ . Additionally, the creation of  $\text{ZnO}/\text{SmMnO}_3$  heterojunction free of any impurities is clearly demonstrated by morphological and analytical analysis. The current study illustrates a straightforward and sophisticated method for designing heterojunction photocatalysts at the hexane-water interface [31]. Yoki Yulizar et al. claims that new strategies for using materials to address

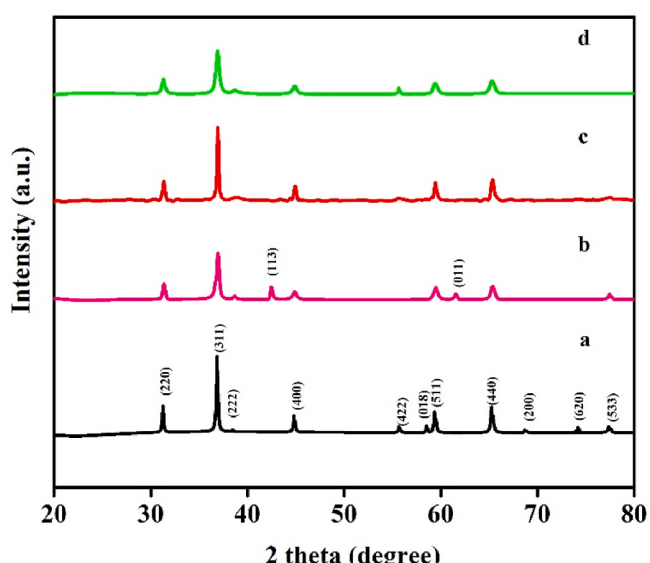


**Fig. 2.** XRD patterns of Tea extract (a), Wine (b), Honey (c), and Cow urine (d) fueled  $\text{Co}_3\text{O}_4$  nanoparticles.

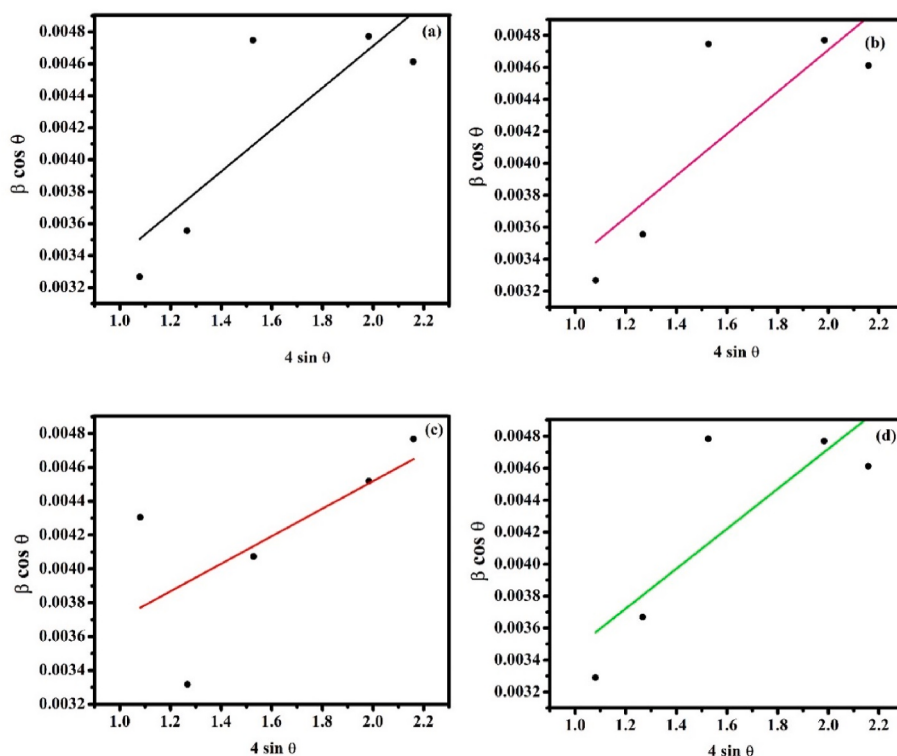


**Fig. 3.** WH plot of green synthesized  $\text{Co}_3\text{O}_4$  nanoparticles: Tea extract (a), Wine (b), Honey (c), and Cow urine (d). (For interpretation of the references to colour in this figure legend, the reader is referred to the Web version of this article.)

environmental problems have emerged all around the world. For instance, water purification has advanced significantly since it is in line with Sustainable Development Goal access to clean water and sanitation. Due to the scarcity of renewable resources, these concerns have become crucial study topics in the past ten years, especially the usage of green photocatalyst. So they describe a novel high-speed stirring method that uses *Annona muricata* L. leaf extracts (AMLE) to modify titanium dioxide with yttrium manganite ( $\text{TiO}_2/\text{YMnO}_3$ ). To speed up the photocatalytic performance for the breakdown of malachite green in aqueous media,  $\text{YMnO}_3$  incorporation in the presence of  $\text{TiO}_2$  was added. The bandgap energy of  $\text{TiO}_2$  after  $\text{YMnO}_3$  alteration fell dramatically from 3.34 to 2.38 eV, with the greatest rate constant ( $k_{app}$ ) of  $2.275 \times 10^{-2} \text{ min}^{-1}$ . Surprisingly, under visible light illumination,  $\text{TiO}_2/\text{YMnO}_3$  had an exceptional photodegradation efficiency of 95.34%, which was 1.9-fold better than that of  $\text{TiO}_2$ . The creation of a  $\text{TiO}_2/\text{YMnO}_3$  heterojunction, a reduced optical band gap, and improved charge carrier separation are all credited with the increased photocatalytic activity. The main scavenger species that contributed significantly to the photodegradation of malachite green were  $\text{H}^+$  and  $\text{O}_2^-$ . Furthermore, the photocatalytic reaction of  $\text{TiO}_2/\text{YMnO}_3$  exhibits

exceptional stability across five cycles without noticeably losing its efficiency. Their work gives a fresh knowledge of the environmentally friendly building of a novel  $\text{TiO}_2$ -based  $\text{YMnO}_3$  photocatalyst for use in water purification, notably in the degradation of organic dyes, with outstanding efficiency in the visible range [32]. Ivan Halomoan et al. synthesized a polar precursor solution and non-polar hexane fraction of *Acmella uliginosa* leaf extract (AUE) were used to create  $\text{CuO-Gd}_2\text{Ti}_2\text{O}_7$  in a two-phase system. In order to create  $\text{CuO-Gd}_2\text{Ti}_2\text{O}_7$ , the secondary metabolites in AUE are crucial. Compared to  $\text{Gd}_2\text{Ti}_2\text{O}_7$ , the optical bandgap for  $\text{CuO-Gd}_2\text{Ti}_2\text{O}_7$  decreased from 3.68 to 1.78 eV. Malachite green (MG) degradation under visible light exposure was examined using photocatalytic activity. After 90 min of illumination,  $\text{CuO-Gd}_2\text{Ti}_2\text{O}_7$  demonstrated MG deterioration at an 88.60% rate, which was 1.9 times greater than MG degradation over  $\text{Gd}_2\text{Ti}_2\text{O}_7$ . After being decorated with  $\text{CuO}$ ,  $\text{Gd}_2\text{Ti}_2\text{O}_7$  has a shorter optical bandgap and is therefore more effective in the visible spectrum, which may account for the increased photocatalytic activity. In order to prepare  $\text{CuO-Gd}_2\text{Ti}_2\text{O}_7$  as a prospective candidate with strong photocatalytic activity for the degradation of malachite green under visible light illumination, this research offers a unique technique [33]. Using *Muntingia calabura* L.

**Table 1**  
Structural parameters, shape and particle stability green synthesized of  $\text{Co}_3\text{O}_4$  nanoparticles.

Samples	$D_{\text{XRD}}$ (nm)	$D_{\text{TEM}}$ (nm)	dislocation density $\delta \times 10^{-3}$ ( $\text{nm}^{-2}$ )	Elastic Strain; $\varepsilon = \beta/2\cot\theta(x10^{-3})$	W-H Plot		Shape	Particle stability (mV)
					$\beta \cos\theta$	$4\sin\theta$		
a	31.256	32.7715	0.935765	0.001096182	0.004190468	1.60185077	Mushroom like structure	-20.2
b	30.4744	29.956	2.620068	0.002190677	0.008139095	1.603812448	Rice like structure	-12.6
c	31.214	31.205	0.929492	0.001085141	0.004196386	1.604039364	Mushroom like structure	-14.4
d	22.948	23.48	2.610388	0.002546913	0.009840524	1.602715664	Cluster pore-like structure	-15.4

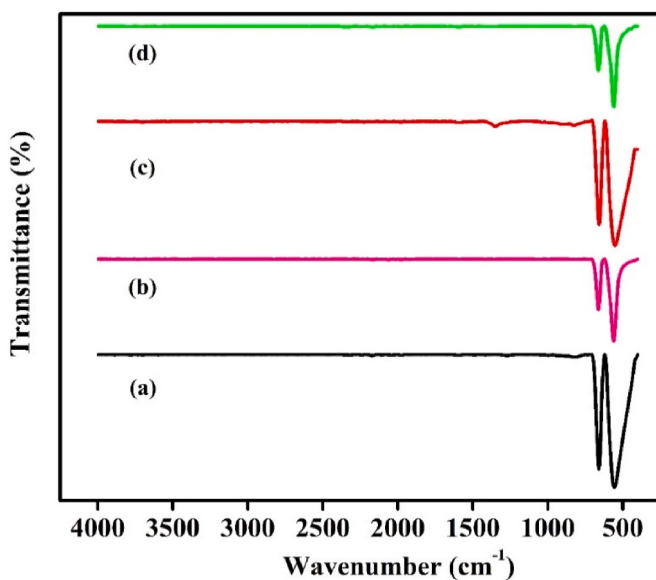


**Fig. 4.** FTIR spectra of green synthesized  $\text{Co}_3\text{O}_4$  nanoparticles: Tea extract (a), Wine (b), Honey (c), and Cow urine (d). (For interpretation of the references to colour in this figure legend, the reader is referred to the Web version of this article.)

leaf extract (MCE), Yoki Yulizar et al. successfully built a  $\text{SnWO}_4/\text{ZnO}$  heterostructure. We performed phytochemical experiments to qualitatively identify the existence of secondary metabolites that are crucial for the synthesis of  $\text{SnWO}_4/\text{ZnO}$ , such as alkaloids, saponins, flavonoids, and tannins. Under visible light irradiation, the photocatalytic activities of pure  $\text{SnWO}_4$ , pure  $\text{ZnO}$ , and  $\text{SnWO}_4/\text{ZnO}$  heterostructure were assessed for the breakdown of methylene blue (MB). The adsorption impact of  $\text{SnWO}_4/\text{ZnO}$  was also investigated in order to examine the photocatalytic activity of  $\text{SnWO}_4/\text{ZnO}$  heterostructure in the visible range. In comparison to pure  $\text{SnWO}_4$  and  $\text{ZnO}$ , which exhibit degradation percentages of 69.48 and 40.41%, respectively, the  $\text{SnWO}_4/\text{ZnO}$  heterostructure exhibits the highest degradation percentage of 82.86%

during 120 min [34]. The green approach was used by Adistyta Maulidya et al. to create unique  $\text{Ce}_2\text{Zr}_2\text{O}_7-\text{TiO}_2$  utilizing Annona Squamosa L. peel extract (ASE). Alkaloids are present in ASE and act as capping and hydrolyzing agents in the production of  $\text{Ce}_2\text{Zr}_2\text{O}_7-\text{TiO}_2$ . To clarify the vibrational, optical, structural, morphological, elemental composition, and photocatalytic properties of  $\text{Ce}_2\text{Zr}_2\text{O}_7-\text{TiO}_2$ , several characterizations were carried out. Under irradiation visible light, the photocatalytic activity of  $\text{TiO}_2$ ,  $\text{Ce}_2\text{Zr}_2\text{O}_7$ , and  $\text{Ce}_2\text{Zr}_2\text{O}_7-\text{TiO}_2$  was assessed for the destruction of methylene blue. In comparison to  $\text{TiO}_2$  and  $\text{Ce}_2\text{Zr}_2\text{O}_7$ ,  $\text{Ce}_2\text{Zr}_2\text{O}_7-\text{TiO}_2$  had a greater degradation percentage. Due to improved visible light absorption and a low rate of electron-hole recombination,  $\text{Ce}_2\text{Zr}_2\text{O}_7$  modification of  $\text{TiO}_2$  increased the photocatalytic activity [35]. In order to fabricate semiconductor electrodes that give higher photoelectrochemical (PEC) performance in the water-splitting reaction, Dewangga Oky Bagus Apriandana et al. developed a macroporous structure of conductive substrates with huge surface areas. In this study, a Ti-doped  $\text{Fe}_2\text{O}_3$  photoanode was made using a hydrothermal approach with a two-step annealing treatment in argon using three-dimensional (3D) titanium microfibre feeling (Ti felt) as a conductive substrate. Ti felt had a loading amount of  $\text{Fe}_2\text{O}_3$  that was 2–5 times higher than that of traditional two-dimensional (2D) substrates, such as fluorine-doped tin oxide (FTO)-coated glass and Ti sheets, for a comparable substrate geometric area.  $\text{Fe}_2\text{O}_3$  was less thick on the Ti felt (0.6 m) than it was on the 2D substrates. Compared to FTO/Ti- $\text{Fe}_2\text{O}_3$  and Ti-sheet/Ti- $\text{Fe}_2\text{O}_3$ , Ti-doped  $\text{Fe}_2\text{O}_3$  on Ti felt (Ti-feeling/Ti- $\text{Fe}_2\text{O}_3$ ) has a greater photocurrent density. The donor density of Ti-felt/Ti- $\text{Fe}_2\text{O}_3$  ( $8.58 \text{ } 10^{21} \text{ cm}^3$ ) was more than 10 times greater than that of FTO/Ti- $\text{Fe}_2\text{O}_3$  and Ti-sheet/Ti- $\text{Fe}_2\text{O}_3$ , according to a Mott-Schottky study [36]. Cobalt oxide nanoparticles were synthesized in this investigation via burning, with natural fuels including wine, cow urine honey, and tea extract. The interaction between an organic complexing agent and a metal ion, known as chelation, results in the formation of a ring structure that encloses the metal ion. Metals are bound together by organic molecules in solutions or on the surfaces of minerals. Chelation is a term used to describe a type of bonding between ions, molecules, and metal ions. A ligand with multiple bonds and the metal atom at the center must form or be bound by two or more different coordinate bonds. They are often organic substances. In conclusion, natural fuel-mediated combustion refers to the influence of naturally occurring substances on the

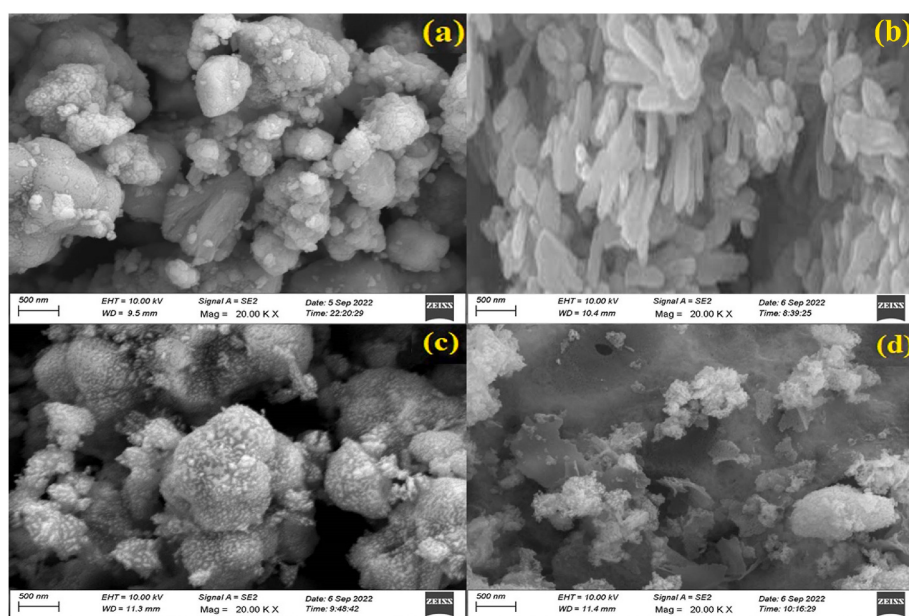


**Fig. 5.** FESEM micrographs of green synthesized  $\text{Co}_3\text{O}_4$  nanoparticles: Tea extract (a), Wine (b), Honey (c), and Cow urine (d). (For interpretation of the references to colour in this figure legend, the reader is referred to the Web version of this article.)

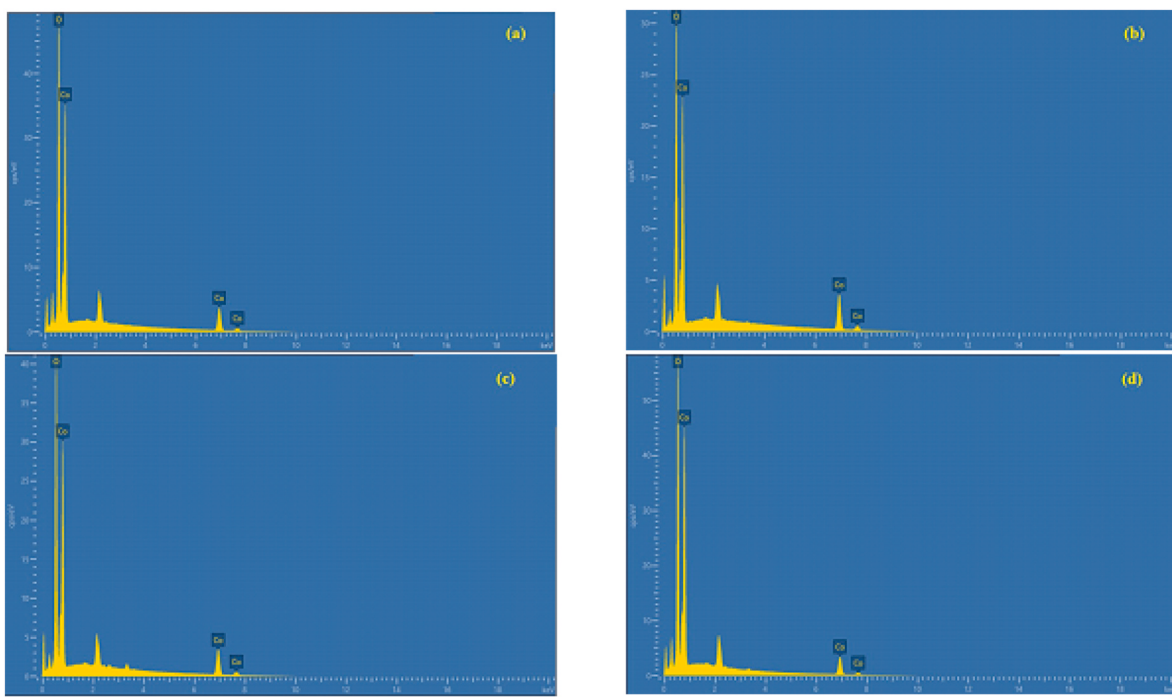


**Fig. 6.** EDX spectra of green synthesized  $\text{Co}_3\text{O}_4$  nanoparticles: Tea extract (a), Wine (b), Honey (c), and Cow urine (d). (For interpretation of the references to colour in this figure legend, the reader is referred to the Web version of this article.)

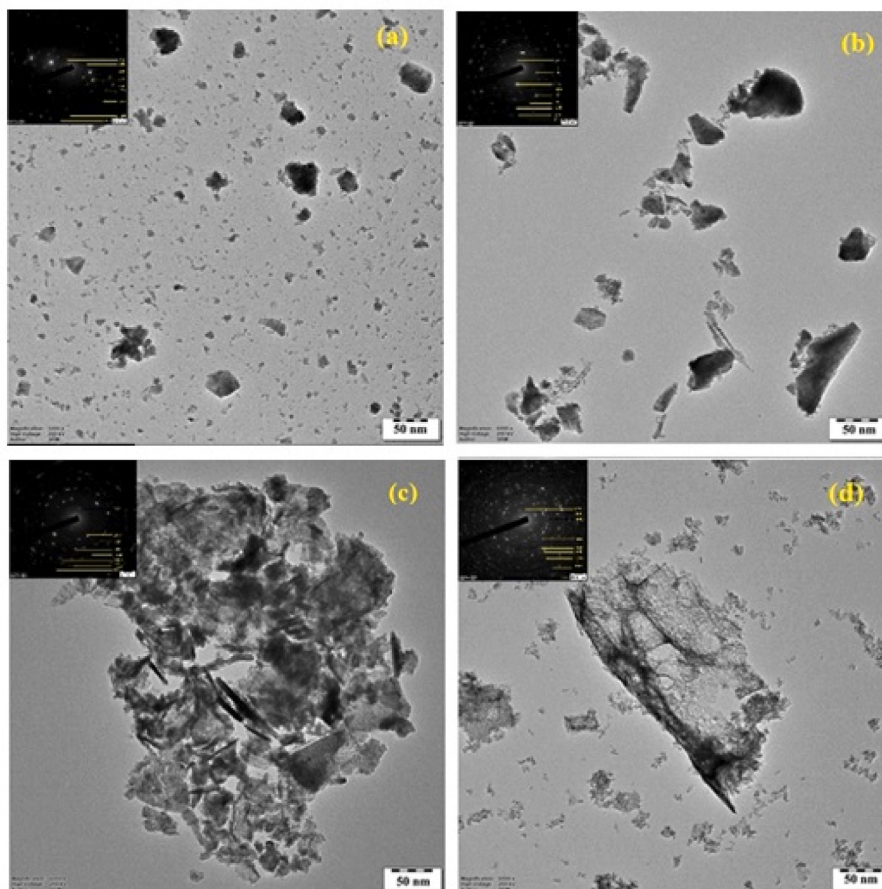


**Fig. 7.** TEM images of green synthesized  $\text{Co}_3\text{O}_4$  nanoparticles: Tea extract (a), Wine (b), Honey (c), and Cow urine (d). (For interpretation of the references to colour in this figure legend, the reader is referred to the Web version of this article.)

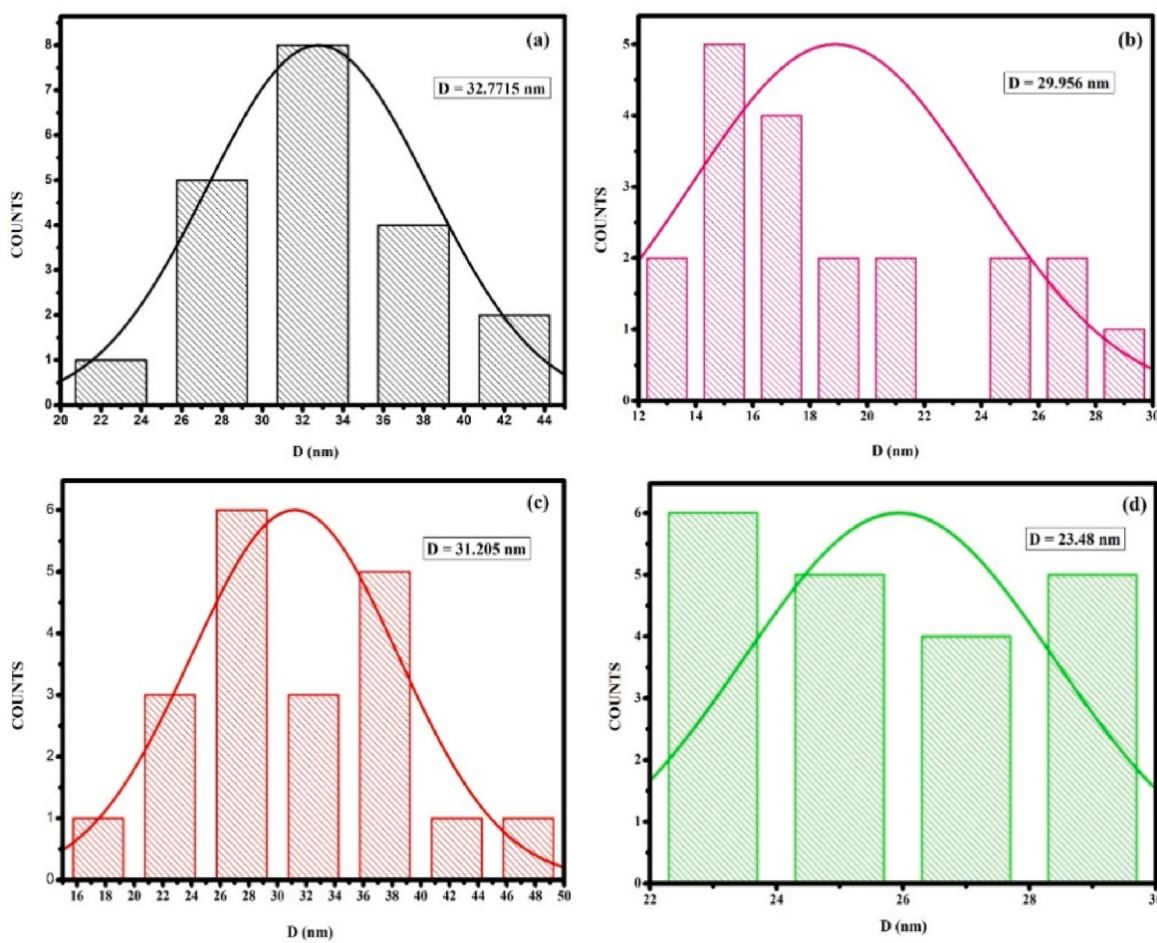


**Fig. 8.** Particle size distribution of green synthesized  $\text{Co}_3\text{O}_4$  nanoparticles: Tea extract (a), Wine (b), Honey (c), and Cow urine (d). (For interpretation of the references to colour in this figure legend, the reader is referred to the Web version of this article.)

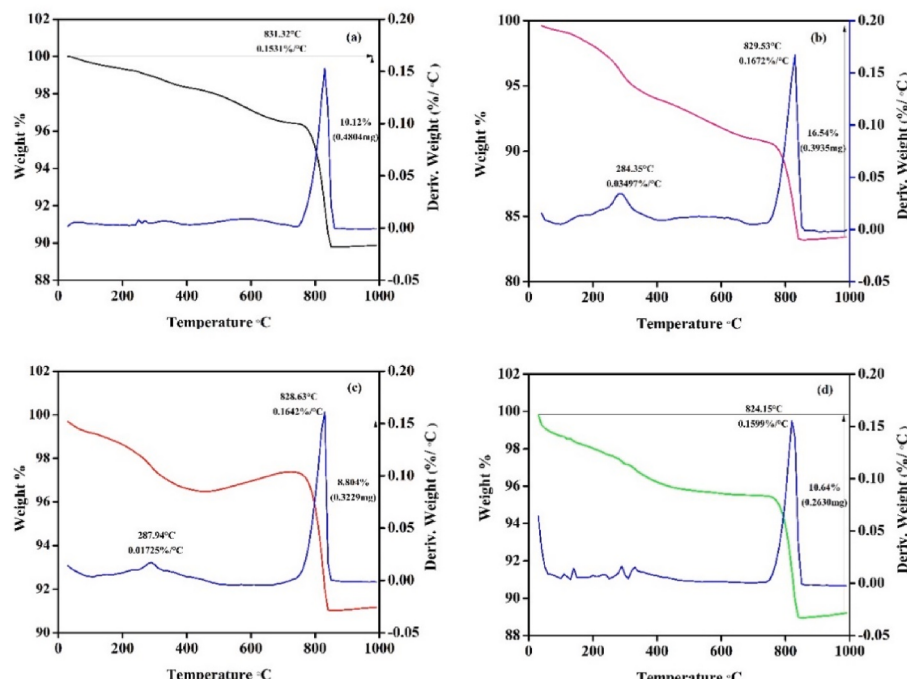


**Fig. 9.** Shows TG/DTA analysis of green synthesized  $\text{Co}_3\text{O}_4$  nanoparticles: Tea extract (a), Wine (b), Honey (c), and Cow urine (d). (For interpretation of the references to colour in this figure legend, the reader is referred to the Web version of this article.)

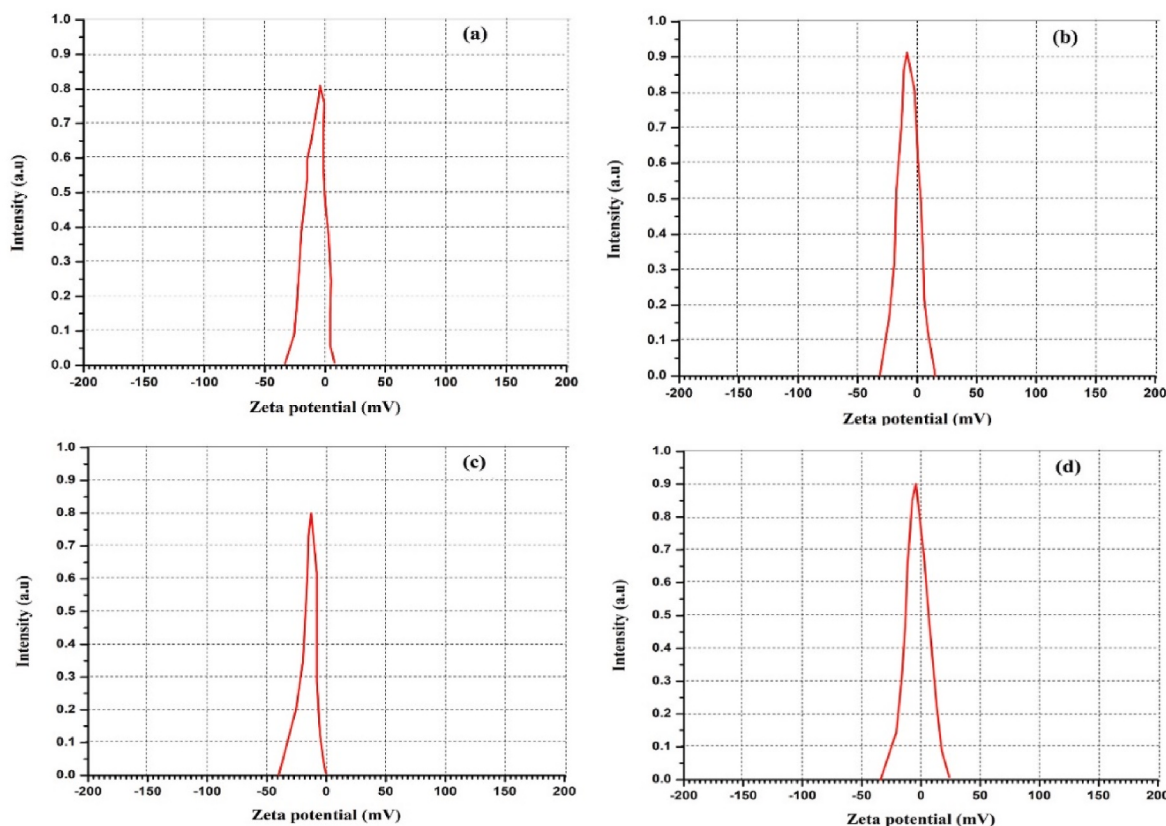


**Fig. 10.** Zeta potential values of green synthesized  $\text{Co}_3\text{O}_4$  nanoparticles: Tea extract (a), Wine (b), Honey (c), and Cow urine (d). (For interpretation of the references to colour in this figure legend, the reader is referred to the Web version of this article.)

combustion process of fuels, which results in altered combustion characteristics and increased efficiency. The chelating process entails the formation of stable complexes between metal ions and chelating agents.  $\text{Co}_3\text{O}_4$  nanoparticles' production, physicochemical characteristics, and biological activities are examined and explored in relation to these natural fuels.

## 2. Experimental procedure

### 2.1. Synthesis method

Nanoparticles of cobalt trioxide ( $\text{Co}_3\text{O}_4$ ) were produced via the deflagration of cobalt nitrate with organic compounds. In addition to analytical grade  $\text{Co}(\text{NO}_3)_2 \cdot 6\text{H}_2\text{O}$  (Merck 99%), key ingredients that are used in the manufacture of  $\text{Co}_3\text{O}_4$  nanoparticles include natural fuels. In the first phase, you will combine 50 ml of water that has been through two distillation processes with 0.5 M of cobalt nitrate. Then, 50 mL of natural fuels were added to the solution in order to start the combustion process. After being stirred for an hour, the solution is dried out by being heated to 100 °C for an hour, and after that, it has the propensity to catch fire.  $\text{Co}_3\text{O}_4$  powder was obtained and then pulverized in a mortar so that a fine powder could be produced. A simplified diagram of the synthesis process is shown in Fig. 1. The prepared samples are named (a) for the Tea extract used, (b) for the wine used, (c) for the Honey used, and (d) for Cow urine used, respectively.

### 2.2. Characterization techniques

With the assistance of a Bruker AXS D8 diffractometer that was outfitted with a  $\text{Cu K}\alpha$  wavelength of 1.5406 Å, analyses of  $\text{Co}_3\text{O}_4$  nanoparticles that were generated from tea extract, wine, honey, and cow urine were successfully carried out. In order to explore the surface

morphology, a Gemini 300 FESEM as well as a JEM-2100 Plus HR-TEM were also used. The thermal investigations were carried out with the assistance of the TG-DTA method that was developed by PerkinElmer. A Horiba SZ100 Zeta Potential Analyzer was utilised for the aim of assessing the degree to which colloidal nanoparticles are stable in order to achieve the aforementioned goal.

### 2.3. Antimicrobial study

At first, we used media for microbial and fungal growth. Among these were Sabouraud Dextrose Agar (SDA) and Muller Hinton Agar (MHA). Antibacterial activity of the produced  $\text{Co}_3\text{O}_4$  NPs was tested on two strains of bacteria: the Gram-positive *Staphylococcus aureus* (ATCC 25923) and the Gram-negative *Pseudomonas aeruginosa* (ATCC 15442). *Candida albicans* (ATCC 10231) and *Aspergillus niger* (ATCC 6275) were tested for their ability to halt fungal growth. The agar diffusion technique was used to measure the antibacterial drugs' efficacy.  $\text{Co}_3\text{O}_4$  was initially dissolved in DMSO (dimethyl sulfoxide) for this procedure. According to published studies,  $\text{Co}_3\text{O}_4$  NPs have been found in DMSO at 1 mg/ml, 2 mg/ml, and 3 mg/ml. In this particular research endeavour, the antifungal and antibacterial medicines fluconazole and streptomycin were utilised respectively. Both of these substances were used as the standard positive control for the inhibition at the concentration levels that were described earlier. The DMSO is stored in its own dedicated diffusion hole, which bears the designation 'negative control' (NC). DMSO does not appear to have an effective inhibitory zone that may be observed. Because of this, it has been demonstrated that DMSO did not possess any particular antibacterial properties, and that  $\text{Co}_3\text{O}_4$  NPs were the only factor responsible for the inhibition. The results of the experiment, which was carried out three times, are presented here as the mean plus the standard error.

### 3. Results and discussion

#### 3.1. XRD studies

**Fig. 2** illustrates the X-ray diffraction (XRD) peaks resulting from the  $\text{Co}_3\text{O}_4$  nanoparticles synthesized using the aforementioned natural fuels. The identification of diffraction planes (2 2 0), (3 1 1), (2 2 2), (4 0 0), (4 2 2), (5 1 1), (4 4 0), (6 2 0), and (5 3 3) in all four samples provides strong evidence for the presence of a cubic spinel structure. This finding is consistent with the information reported in JCPDS (43–1003). Based on the remarkably pronounced peaks seen, it can be inferred that the  $\text{Co}_3\text{O}_4$  nanoparticles synthesized possess a significant level of crystallinity. Throughout the entirety of the combustion process, it is imperative to ensure the efficient chelation of all organic molecules. The crystallite size was determined and approximated using the William-Hall (W-H) plot method, a widely employed technique. The crystal characteristics ascertained by the formula are presented in **Table 1**. The influence of different fuels is evident in the variations seen in the crystallographic properties of the sample generated through the utilization of several natural fuel sources (see **Fig. 3**).

#### 3.2. FT-IR analysis

**Fig. 4** depicts the outcomes of the FTIR tests conducted on samples of compounds a, b, c, and d. In the FTIR spectra of  $\text{Co}_3\text{O}_4$  nanoparticles, it can be seen that a significant absorption band appears at  $567 \text{ cm}^{-1}$ , as well as  $661 \text{ cm}^{-1}$ . It was shown that the absorption band with a frequency of  $567 \text{ cm}^{-1}$  corresponds to the Co–O stretching vibration mode, whereas the band with a frequency of  $661 \text{ cm}^{-1}$  is connected with the

O–Co–O bond bridging vibration [37]. There are no vibrations other than those of  $\text{Co}_3\text{O}_4$ , as shown by the fact that the interactions between organic molecules are exceedingly weak and unstable. This is evidence that there are no other vibrations. Because the FTIR results coincide with the XRD and EDAX readings, we are in a position to demonstrate that the  $\text{Co}_3\text{O}_4$  we have access to is of the highest possible quality.

#### 3.3. Surface and elemental analysis

In **Fig. 5**, FE-SEM and EDAX photos of the samples were displayed for viewing. The morphologies of each sample were analyzed and compared. Overall the even distribution of uniform surface morphology provides optimum charge distribution which is very much required for charge distribution. Among these, tea extract is the most effective green fuel for combustion and also functions rather well as a chelating agent. The mushroom-like agglomeration of  $\text{Co}_3\text{O}_4$  NPs triggered by tea extract can be seen in the image obtained by scanning electron microscopy. Honey was found to be the product that was the second most reliable chelating agent due to the gluconic acid [38]. The elemental analysis revealed that the nanoparticles possessed satisfactory stoichiometric amounts of cobalt and oxide. It has been determined that almost all of the organic agents were consumed by combustion due to the fact that the EDAX plots have essentially no carbon peaks. During the FTIR test, the carbon-based compounds did not show any signs of vibrations. This leads one to believe that the organic surfactants were responsible for the efficient burning. Not only did they not produce any combustion waste, but they also had no influence on the properties of the prepared nanoparticles (see **Fig. 6**).

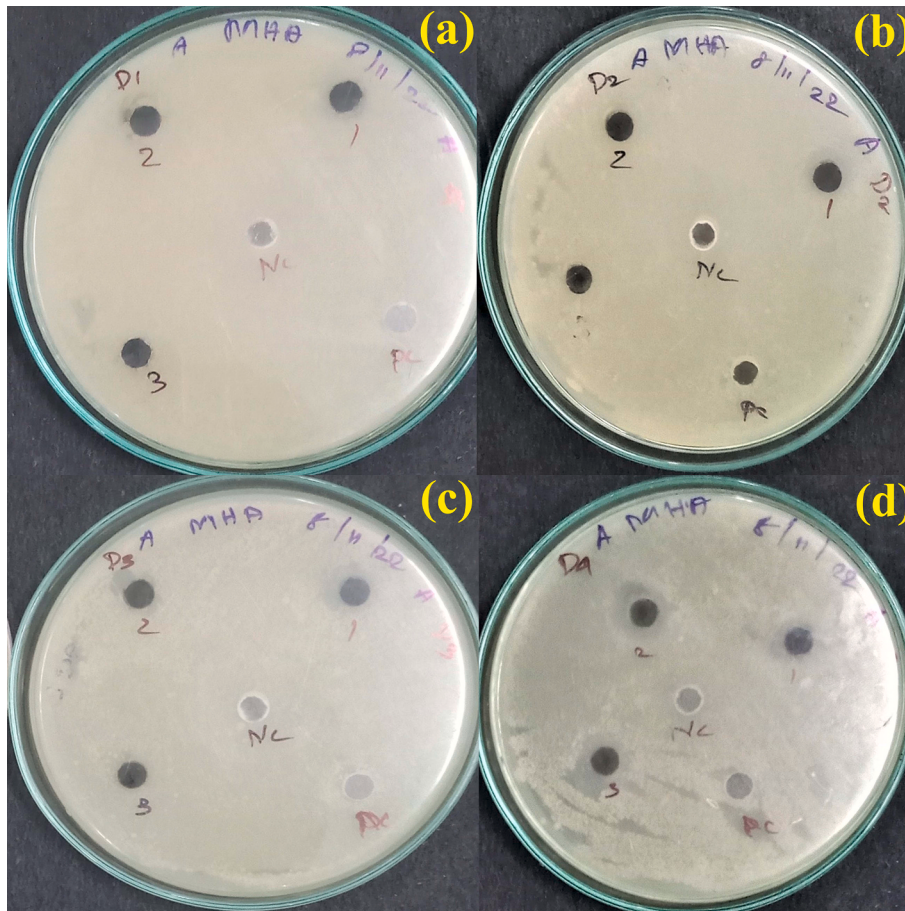


**Fig. 11.** Anti-bacterial test against *Staphylococcus aureus* - Gram-positive bacteria using green synthesized  $\text{Co}_3\text{O}_4$  nanoparticles: Tea extract (a), Wine (b), Honey (c), and Cow urine (d). (For interpretation of the references to colour in this figure legend, the reader is referred to the Web version of this article.)

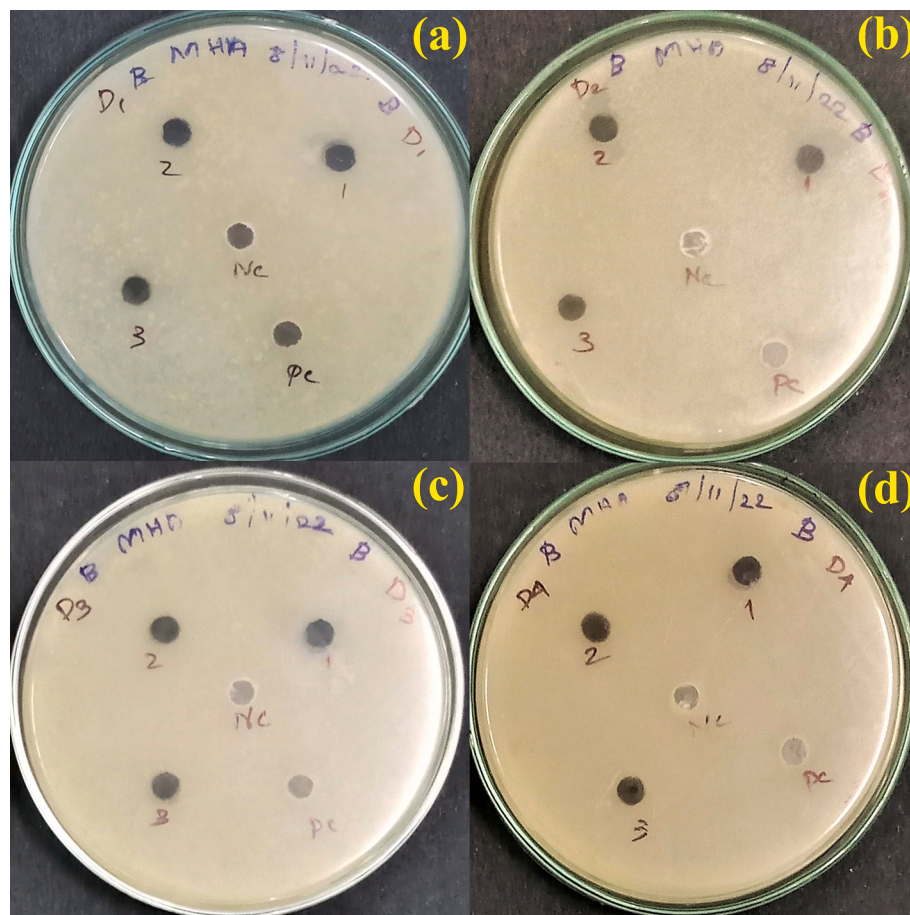


**Fig. 12.** Anti-bacterial test against *Pseudomonas aeruginosa* - Gram-negative bacteria using green synthesized  $\text{Co}_3\text{O}_4$  nanoparticles: Tea extract (a), Wine (b), Honey (c), and Cow urine (d). (For interpretation of the references to colour in this figure legend, the reader is referred to the Web version of this article.)

#### 3.4. TEM analysis

The TEM and SAED patterns of each and every sample were displayed in Fig. 7. Fig. 8 depicts the distribution of particle sizes including the average particle size. There was just a trace amount of particle aggregation visible in any of the samples. It was discovered that the TEM pictures and the SEM morphologies had a strong correlation with one another. Images taken using a transmission electron microscope show that the fuels also form nanoscale particles, which act as an effective capping agent and prevent agglomeration. In general, we are able to draw the conclusion that increasing the supply of fuel can improve morphology since it has a tendency to withstand combustion for a longer period of time and improves the efficiency of the reaction. The images obtained from the TEM confirmed that the fuels also form nanoscale particles, which can act as an effective capping agent to stop agglomeration from happening. By increasing the amount of fuel available, combustion may be made to continue for longer periods of time, which in turn speeds up reaction process. This gives us reason to assume that morphology can be improved. There is a consistent pattern of particle size distribution throughout all of the samples, and the average particle size has a strong correlation with the results of the XRD particle size computation.

#### 3.5. Thermal analysis

The TG/DTA was examined in an atmosphere consisting of nitrogen at temperatures ranging from 0 to 1000° Celsius. The results of the analysis are presented in Fig. 9. In aggregate, each sample lost weight in

a manner that was progressive and comparable. It was noted that all of the samples experienced a normal endothermic reaction, and that they lost a consistent amount of weight all the way up to 1000 °C. The range of melting points for all of the samples was between 828 and 830 °C [39]. Even after being heated to 1000 °C, the weight of the wine- and cow-urine-assisted  $\text{Co}_3\text{O}_4$  NPs was found to have been retained at 16.54% and 10.64%, respectively. It was shown that honey aided  $\text{Co}_3\text{O}_4$  NPs had a greater stability than other samples.

#### 3.6. Zeta potential

The surface loads of the individual particles in a colloidal suspension or nanoparticle suspension can have an effect on the suspension as a whole. This applies to both centralised and decentralised structures. Some applications necessitate stability, therefore investigating how suspension properties impact electrostatic stabilisation is crucial. This is due to the fact that stability is required by some applications. The particle colloidal stability of  $\text{Co}_3\text{O}_4$  nanoparticles was analyzed and the zeta potential values are shown in Fig. 10. The negative charges for  $\text{Co}_3\text{O}_4$  nanoparticles for all four samples a, b, c and d are determined to be approximately  $-20.2$  mV,  $-12.6$  mV,  $-14.4$  mV, and  $-15.4$  mV, respectively. The  $\text{Co}_3\text{O}_4$  NPs driven by tea extract have a surface that is more uniform, which contributes to their increased stability as colloidal particles. As a consequence of this, these particles will have a reduced propensity to bunch together and will remain in their colloidal state for a long time while keeping their initial size. This is the most important characteristic that needs to be present for NPs to be effective antibacterial agents.

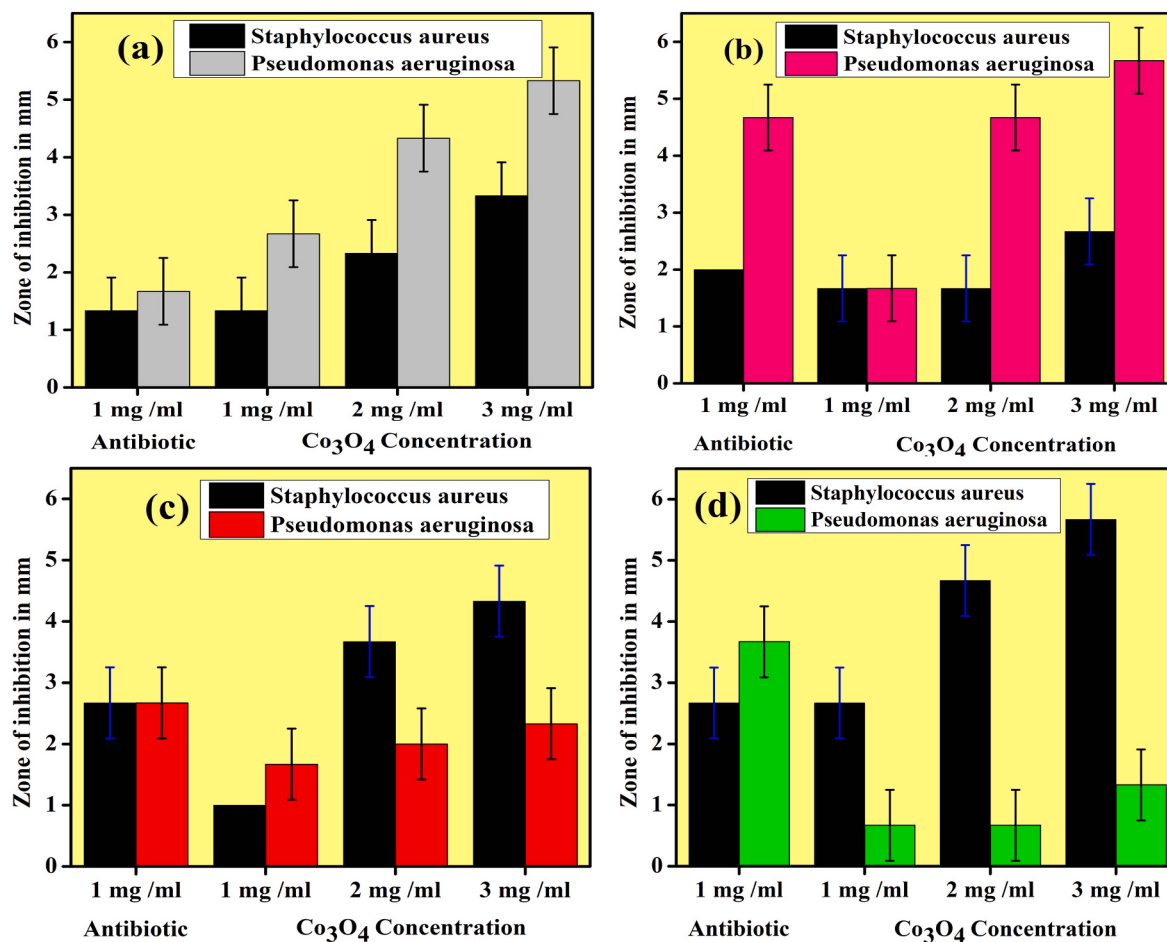


**Fig. 13.** Bar diagram of Anti-bacterial test using green synthesized Co<sub>3</sub>O<sub>4</sub> nanoparticles: Tea extract (a), Wine (b), Honey (c), and Cow urine (d). (For interpretation of the references to colour in this figure legend, the reader is referred to the Web version of this article.)

### 3.7. Anti-bacterial activity

For testing the effectiveness of Co<sub>3</sub>O<sub>4</sub> nanoparticles as an antibacterial agent against Gram-positive and Gram-negative bacteria, respectively, the agar well diffusion method and the Muller Hinton Agar (MHA) were utilised. When introducing the samples into the dispersed hole, doses of 1, 2, and 3 were applied. The size of the inhibitory zone has been restrained in millimetres after being subjected to incubation for a period of 24 h. In all of the samples, inhibition increases in a linear fashion as concentration increases. The antibacterial impact can be attributed to the increased release of metallic ions as well as the intimate interaction that occurs between nanoparticles and the membrane of bacteria. Metallic nanoparticles exert their antibacterial activity by a mechanism that is reliant on their size. This process alters the cell membrane and restricts transport channels, so reducing the bacteria's ability to carry out their function. It has been demonstrated that the ionisation that occurs as a result of the penetration of nanoscale metallic ions into cells results in changes to the intracellular structures, which ultimately leads to the death of the cells [40–42]. Hydrogen peroxide (H<sub>2</sub>O<sub>2</sub>), hydroxyl radicals (OH), superoxide radicals (O), singlet oxygen (O), and hydrogen peroxide (O) are all examples of the short-lived oxidants that generate ROS with several functions [43]. Reactive oxidative species (ROS) are known to cause damage to a wide variety of biomolecules, including proteins, peptidoglycan, messenger RNA, DNA, ribosomes, and cell membranes [44,45]. This can be accomplished by distributing surface charges in an even manner over the surface. In order to achieve this objective, the Zeta potentials of each and every one of synthesized samples were optimised. Co<sub>3</sub>O<sub>4</sub> nanoparticles become more

effective at preventing the development of bacteria and increasing the size of the inhibition zone as their concentration increases. The microorganisms were grown on a number of different plates, and the results of the cultivation process are presented in Figs. 11 and 12, which illustrate, respectively, the suppression of gram-positive and gram-negative bacteria. Fig. 13 displays a plot of antibacterial efficacy for your viewing pleasure. Both bacteria were revealed to be significantly thwarted by the presence of Co<sub>3</sub>O<sub>4</sub> nanoparticles. Because of this, the particles are able to break through the peptidoglycan layers that make up the cell wall.

### 3.8. Anti-fungal activity

Using the agar well diffusion technique the anti-fungal activity of Co<sub>3</sub>O<sub>4</sub> NPs against *Aspergillus niger* and *Candida albicans* were studied. The samples (1, 2, and 3 mg/ml, respectively) were poured into the diffusion well. Following a full day of incubation, we determined the diameter of the inhibitory zone to be one mm in increments. Each individual sample is capable of inhibiting both fungi. Figs. 14 and 15 depict the inhibitory zone in its various forms. A variety of fungal cultures were distributed across a number of plates. The graphic representation of the zone of inhibition can be found in Fig. 16. The cell membranes of fungi consist of protein molecules that are encased in a lipid bilayer. The creation of the sterol ergosterol, which is necessary for maintaining the integrity of membranes, is the responsibility of the enzyme known as 14-Demethylase. Cell membranes include a glucan synthase complex, which is responsible for the synthesis of 1,3-glucan chains. The strength of cell wall comes from longer glucan chains that are cross-linked with chitin at regular intervals. The majority of

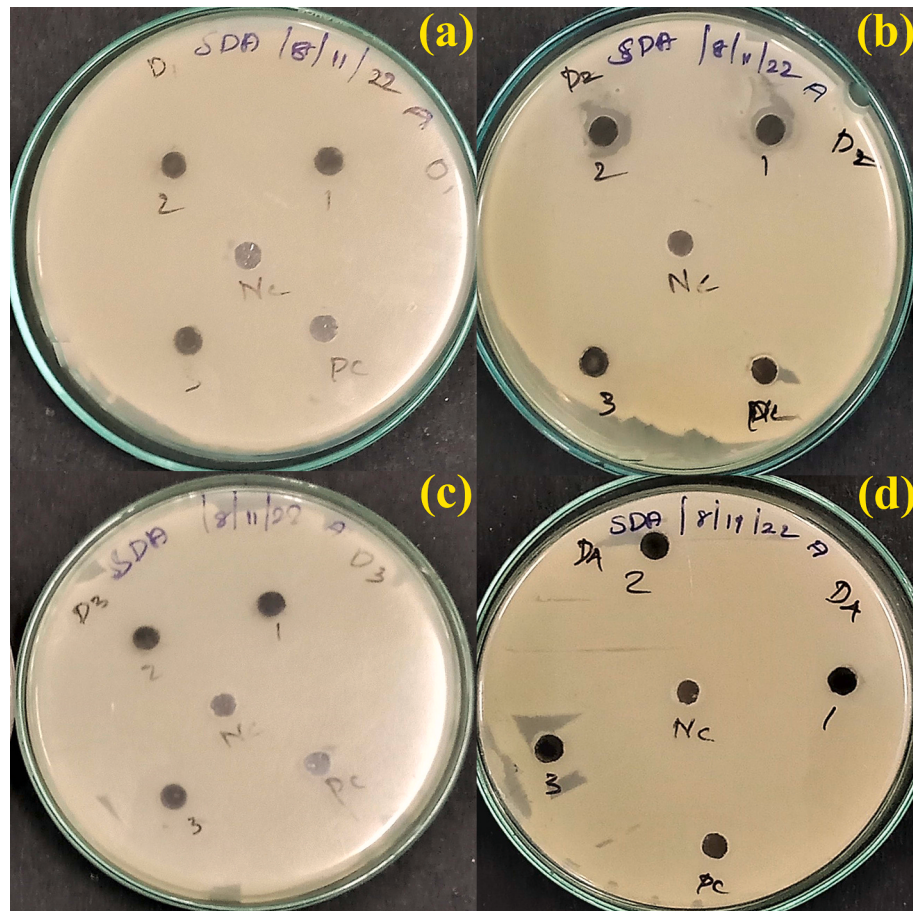


**Fig. 14.** Anti-fungal test against *Aspergillus niger* - Mould fungi using green synthesized  $\text{Co}_3\text{O}_4$  nanoparticles: Tea extract (a), Wine (b), Honey (c), and Cow urine (d). (For interpretation of the references to colour in this figure legend, the reader is referred to the Web version of this article.)

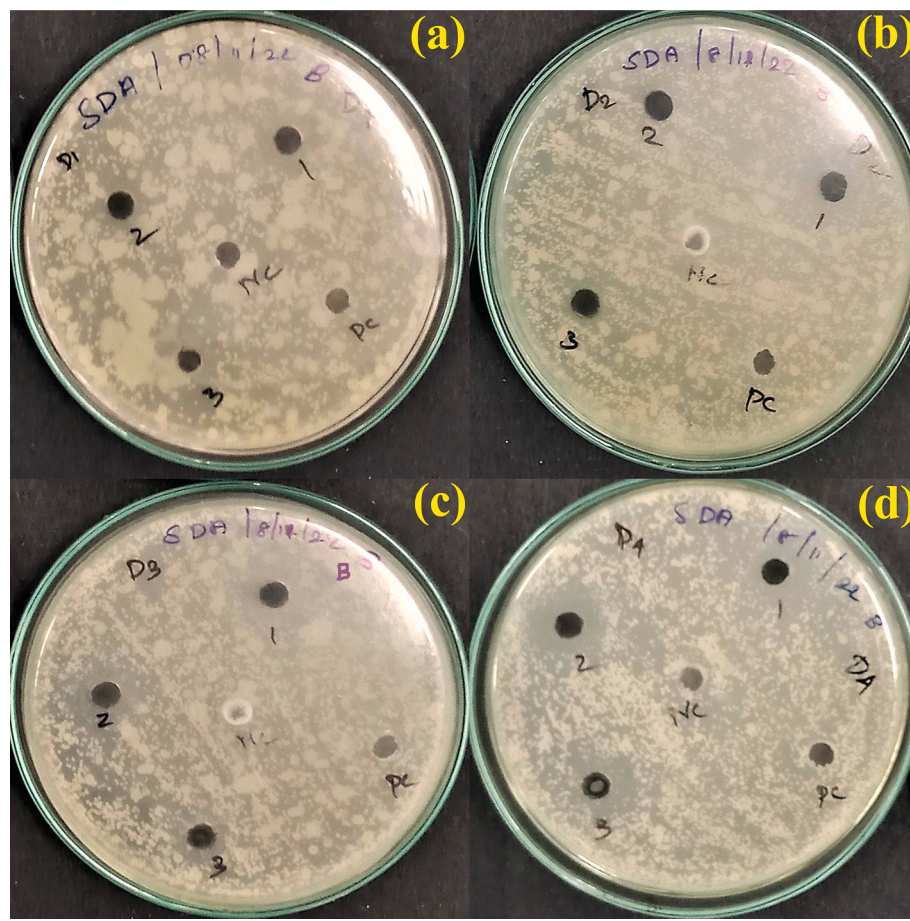


**Fig. 15.** Anti-fungal test against *Aspergillus niger* - Yeast fungi using green synthesized  $\text{Co}_3\text{O}_4$  nanoparticles: Tea extract (a), Wine (b), Honey (c), and Cow urine (d). (For interpretation of the references to colour in this figure legend, the reader is referred to the Web version of this article.)

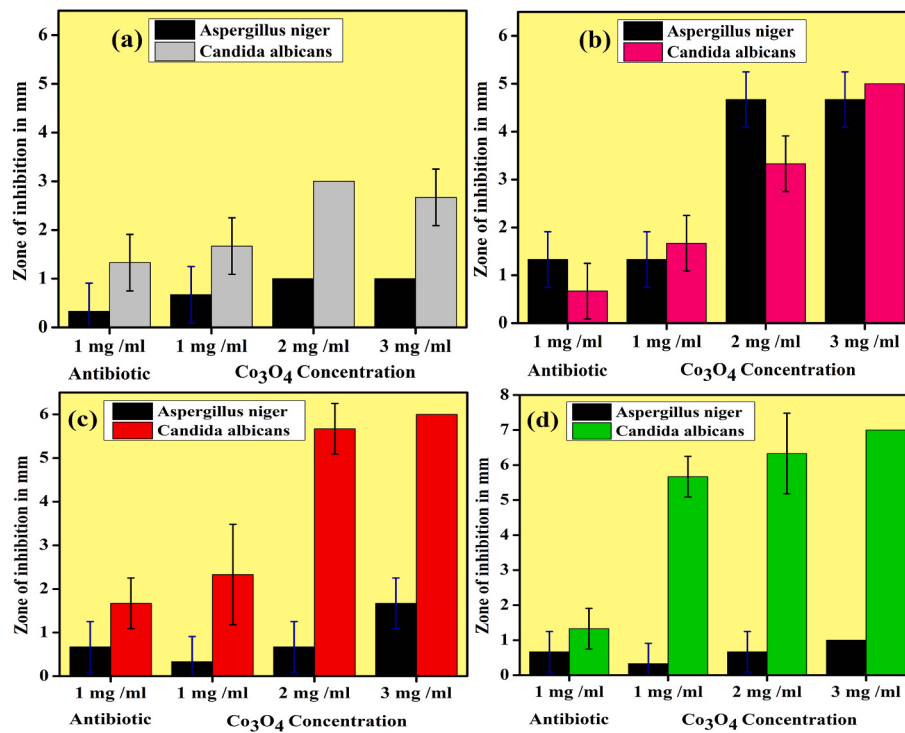


**Fig. 16.** Bar diagram of Anti-Fungal test using green synthesized  $\text{Co}_3\text{O}_4$  nanoparticles: Tea extract (a), Wine (b), Honey (c), and Cow urine (d). (For interpretation of the references to colour in this figure legend, the reader is referred to the Web version of this article.)

antifungal drugs accomplish their primary objective, which is to bind to ergosterol and stop it from becoming methylated. It has been discovered that exposure to  $\text{Co}_3\text{O}_4$  nanoparticles results in an increase in the permeability of cells and a reduction in the accumulation of ergosterol on the surfaces of cell walls. Nanoparticles that have a charge distribution that is uniform have a reaction with ergosterol that stops the process and depletes the cell fluids. When the temperature rises, an increasing number of individual cobalt ions are able to break through the cell wall and react with ergosterol. This happens more frequently as the temperature rises. The end outcome is an antifungal action that has been catalyzed.

#### 4. Conclusion

The synthesis of cobalt oxide ( $\text{Co}_3\text{O}_4$ ) nanoparticles was conducted using a straightforward combustion procedure that utilised natural fuels. Subsequently, an investigation was carried out to analyze the structural, morphological, thermal, and antibacterial characteristics of the generated nanoparticles. Based on X-ray diffraction (XRD) studies, it has been shown that each specimen possesses a cubic crystalline structure. The  $\text{Co}_3\text{O}_4$  nanoparticles were synthesized using naturally occurring macromolecules including cow urine, honey, wine, and tea extract. The resulting nanoparticles exhibited crystallite sizes in the range between 22 and 31 nm. Based on the findings from FESEM and EDAX investigations, it was seen that the products exhibited stoichiometric geometries resembling rice grains, mushrooms, and cluster cavities. Additionally, the EDX analysis showed the existence of both cobalt (Co) and oxygen (O) elements within the samples. The Fourier Transform Infrared (FTIR) image provided evidence of the existence of diverse phytochemicals on the surface. Additionally, the bands observed at 400 and  $630 \text{ cm}^{-1}$  indicated the presence of unique Co–O connections. The sizes of crystallites and TEM particles have a similar magnitude in terms of their diameters. The thermal characteristics of  $\text{Co}_3\text{O}_4$  nanoparticles, which have been produced using various natural fuels, exhibit significant reductions in weight. The investigation of the colloidal stability of the particle has been conducted. This finding provides confirmation that the utilization of natural resources has a direct impact on the stability of particles. The antibacterial and antifungal properties of  $\text{Co}_3\text{O}_4$  nanoparticles produced using green methods were assessed against two different types of bacteria, namely *Staphylococcus aureus* (Gram-positive) and *Pseudomonas aeruginosa* (Gram-negative), as well as two fungi, *Candida albicans* and *Aspergillus niger*. Recent research findings have revealed that synthesized  $\text{Co}_3\text{O}_4$  nanoparticles exhibit a significant inhibitory effect on the proliferation of both microbial and fungal organisms.

#### Declaration of competing interest

There is no Conflict of Interest.

#### Acknowledgments

The authors extend their appreciation to the Deanship of Scientific Research at King Khalid University for funding this work through large group Research Project under grant number RGP2/325/44.

#### References

- [1] Yinghua Qiu, Yunpeng Wang, Controllable synthesis of porous  $\text{Co}_3\text{O}_4$  nanorods and their ethanol-sensing performance, *Ceram. Int.* 48 (20) (2022) 29659–29668.
- [2] Lizhi Xiong, Teng Yao, Yuxian Wu, Jiajian Wang, Ziqiang He, Large-scale synthesis of aligned  $\text{Co}_3\text{O}_4$  nanowalls on nickel foam and their electrochemical performance for Li-ion batteries, *Ceram. Int.* 40 (10) (2014) 15561–15568.
- [3] Saeed Gharpure, Aman Akash, Balaprasad Ankamwar, A review on antimicrobial properties of metal nanoparticles, *J. Nanosci. Nanotechnol.* 20 (6) (2020) 3303–3339.
- [4] Zifeng Wang, Xing Zhang, Yan Sun, Hui Zhang, Congliang Wang, Anjian Xie, Facile synthesis and electrochemical performance of nitrogen-doped porous hollow coaxial carbon fiber/ $\text{Co}_3\text{O}_4$  composite, *Ceram. Int.* 44 (6) (2018) 5848–5854.
- [5] Piyal Mondal, A. Anweshan, Mihir Kumar Purkait, Green synthesis and environmental application of iron-based nanomaterials and nanocomposite: a review, *Chemosphere* 259 (2020), 127509.
- [6] Wanli Zhang, Weibo Jiang, Antioxidant and antibacterial chitosan film with tea polyphenols-mediated green synthesis silver nanoparticle via a novel one-pot method, *Int. J. Biol. Macromol.* 155 (2020) 1252–1261.
- [7] Muhammad Aadil, Sonia Zulfiqar, Muhammad Farooq Warsi, Philips O. Agboola, Imran Shakir, Muhammad Shahid, Najeeb Fuad Al-Khalili, Mesoporous and macroporous Ag-doped  $\text{Co}_3\text{O}_4$  nanosheets and their superior photo-catalytic properties under solar light irradiation, *Ceram. Int.* 47 (7) (2021) 9806–9817.
- [8] Yirong Zhao, Ying Liu, Jingwei Du, Xudong Zhang, Jinyuan Zhou, Xiaopeng Li, Caixia Wu, Ziran Zhu, Erqing Xie, Xiaojun Pan, Facile synthesis of interconnected carbon network decorated with  $\text{Co}_3\text{O}_4$  nanoparticles for potential supercapacitor applications, *Appl. Surf. Sci.* 487 (2019) 442–451.
- [9] Huiyu Chen, Jinpeng Wang, Liao Fan, Han Xingrong, Xu Chunju, Zhang Yanfe, Facile synthesis of porous Mn-doped  $\text{Co}_3\text{O}_4$  oblique prisms as an electrode material with remarkable pseudocapacitance, *Ceram. Int.* 45 (6) (2019) 8008–8016.
- [10] Shiva Bhandari, Boyi Hao, Kevin Waters, Chee Huei Lee, Idrobo Juan-Carlos, Dongyan Zhang, Ravindra Pandey, Yoke Khin Yap, Two-dimensional gold quantum dots with tunable bandgaps, *ACS Nano* 13 (4) (2019) 4347–4353.
- [11] S. Divya, S. Cathrin Lims, M. Manivannan, R. Robert, S. Jerome Das, M. Jose, Impact of amorphous  $\text{SiO}_2$  as shell material on superparamagnetic  $\text{Fe}_3\text{O}_4$  nanoparticles and investigation of temperature and frequency dependent dielectric properties, *J. Alloys Compd.* 919 (2022), 165751.
- [12] Joao Resende, Abderrahime Sekkat, Viet Huong Nguyen, Tomy Chatin, Carmen Jiménez, Mónica Burriel, Daniel Bellet, David Muñoz-Rojas, Planar and transparent memristive devices based on titanium oxide coated silver nanowire networks with tunable switching voltage, *Small* 17 (21) (2021), 2007344.
- [13] Junke Zhu, Wenmao Tu, Hongfei Pan, Heng Zhang, Bin Liu, Yapeng Cheng, Deng Zhao, Haining Zhang, Self-templating synthesis of hollow  $\text{Co}_3\text{O}_4$  nanoparticles embedded in N, S-dual-doped reduced graphene oxide for lithium ion batteries, *ACS Nano* 14 (5) (2020) 5780–5787.
- [14] Pengfei Cheng, Dang Fan, Yinglin Wang, Jianning Gao, Luping Xu, Chen Wang, Li Lv, Li Xu, Bao Zhang, Baijun Liu, Gas sensor towards n-butanol at low temperature detection: hierarchical flower-like Ni-doped  $\text{Co}_3\text{O}_4$  based on solvent-dependent synthesis, *Sensor. Actuator. B Chem.* 328 (2021), 129028.
- [15] Jahdaly Al, Badreah Ali, Ahmed Abu-Rayyan, Mohamed M. Taher, Kamel Shoreir, Photsynthesis of  $\text{Co}_3\text{O}_4$  nanoparticles as the high energy storage material of an activated carbon/ $\text{Co}_3\text{O}_4$  symmetric supercapacitor device with excellent cyclic stability based on a  $\text{Na}_2\text{SO}_4$  aqueous electrolyte, *ACS Omega* 7 (27) (2022) 23673–23684.
- [16] Congcong Lu, Lingran Liu, Yu Yang, Yunping Ma, Luo Qiao, Maiyong Zhu, Recent progress in  $\text{Co}_3\text{O}_4$ -based nanomaterials for supercapacitors, *ChemNanoMat* 9 (5) (2023), e202200537.
- [17] Mohsen Safaei, Mojtaba Taran, Ladan Jamshidy, Mohammad Moslem Imani, Hamid Reza Mozaffari, Roohollah Sharifi, Golshah Amin, Hedaiaj Moradpoor, Optimum synthesis of polyhydroxybutyrate- $\text{Co}_3\text{O}_4$  bionanocomposite with the highest antibacterial activity against multidrug resistant bacteria, *Int. J. Biol. Macromol.* 158 (2020) 477–485.
- [18] Mohamed Abdel Salam, Mostafa R. Abukhadra, Alyaa Adlai, Insight into the adsorption and photocatalytic behaviors of an organo-bentonite/ $\text{Co}_3\text{O}_4$  green nanocomposite for malachite green synthetic dye and Cr (VI) metal ions: application and mechanisms, *ACS Omega* 5 (6) (2020) 2766–2778.
- [19] N.R. Khalid, Areeg Gull, Faisal Ali, M.B. Tahir, T. Iqbal, M. Rafique, Mohammad A. Assiri, Muhammad Imran, Meshal Alzaid, Bi-functional green-synthesis of  $\text{Co}_3\text{O}_4$  NPs for photocatalytic and electrochemical applications, *Ceram. Int.* 48 (21) (2022) 32009–32021.
- [20] S. Akshatha, S. Sreenivasa, L. Parashuram, Fahad A. Alharthi, Chakrapani Rao Tadimety Madhu, Microwave assisted green synthesis of p-type  $\text{Co}_3\text{O}_4$ @Mesoporous carbon spheres for simultaneous degradation of dyes and photocatalytic hydrogen evolution reaction, *Mater. Sci. Semicond. Process.* 121 (2021), 105432.
- [21] Sana Batool, Murtaza Hasan, Momina Dilshad, Ayesha Zafar, Tuba Tariq, Aqeela Shaheen, Rafia Iqbal, et al., Green synthesized  $\text{ZnO-Fe}_2\text{O}_3\text{-Co}_3\text{O}_4$  nanocomposite for antioxidant, microbial disinfection and degradation of pollutants from wastewater, *Biochem. Systemat. Ecol.* 105 (2022), 104535.
- [22] R. Poonguzhal, E. Vandamar, Ranjith Kumar, Ch Srinivas, Mubark Alshareef, Meshari M. Aljohani, Ali A. Keshk, Nashwa M. El-Metwally, N. Arunadevi, Natural lemon extract assisted green synthesis of spinel  $\text{Co}_3\text{O}_4$  nanoparticles for LPG gas sensor application, *Sensor. Actuator. B Chem.* 377 (2023), 133036.
- [23] Qing-Yun Chen, Sajjad U. Haq, Zhong-Hang Xing, Yun-Hai Wang, Temperature effect on green-synthesized  $\text{Co}_3\text{O}_4$  nanoparticle as photocatalyst for overall water splitting, *J. Photon. Energy* 10 (4) (2020), 042006–042006.
- [24] Eneyew Tilahun Bekele, H.C. Murthy, Dhanalakshmi Muniswamy, Yeshehane Adimasu Lemeh, Minale Shegaw Shume, Gezahegn Tadesse Ayanie, Avvaru Praveen Kumar, C.R. Ravikumar, R. Balachandran, Arpita Roy, Solanum tuberosum leaf extract templated synthesis of  $\text{Co}_3\text{O}_4$  nanoparticles for electrochemical sensor and antibacterial applications, *Bioinorgan. Chem. Appl.* (2022) 2022.
- [25] C. Maria Magdalane, K. Kaviyarasu, M.V. Arularasu, K. Kanimozi, G. Ramalingam, Structural and morphological properties of  $\text{Co}_3\text{O}_4$  nanostructures:

- investigation of low temperature oxidation for photocatalytic application for waste water treatment, *Surface. Interfac.* 17 (2019), 100369.
- [26] Ashi Khalil, Nauman Ali, Adnan Khan, Abdullah M. Asiri, Tahseen Kamal, Catalytic potential of cobalt oxide and agar nanocomposite hydrogel for the chemical reduction of organic pollutants, *Int. J. Biol. Macromol.* 164 (2020) 2922–2930.
- [27] Kondaiah Seku, G. Bhagavanth Reddy, Syed Sulaiman Hussaini, Pejjai Babu, Mushtaq Hussain, D. Madhusudan Reddy, Mahmoud AK. Khazaleh, Girija Mangatayaru, An efficient biosynthesis of palladium nanoparticles using Bael gum and evaluation of their catalytic and antibacterial activity, *Int. J. Biol. Macromol.* 209 (2022) 912–922.
- [28] C.T. Anuradha, P. Raji, Facile-synthesis and characterization of cobalt oxide ( $\text{Co}_3\text{O}_4$ ) nanoparticles by using Arishta leaves assisted biological molecules and its antibacterial and antifungal activities, *J. Mol. Struct.* 1262 (2022), 133065.
- [29] C. Arun Paul, E. Ranjith Kumar, J. Suryakanth, A.F. Abd El-Rehim, Structural, microstructural, vibrational, and thermal investigations of NiO nanoparticles for biomedical applications, *Ceram. Int.* 49 (2023) 27230–27246.
- [30] D. Prabaharan, Durai Manoharadoss, K. Sadaiyandi, M. Mahendran, Suresh Sagadevan, Precipitation method and characterization of cobalt oxide nanoparticles, *Appl. Phys. A* 123 (2017) 1–6.
- [31] R.M. Surya, S. Mauliddiyah, D.O.B. Apriandau, Y. Yulizar, SmMnO<sub>3</sub>-decorated ZnO in a hexane-water interface for enhancing visible light-driven photocatalytic degradation of malachite green, *Chemosphere* 304 (2022), 135125.
- [32] Y. Yulizar, Iman Abdullah, Rizki Marcony Surya, Naya Luvy Alifa, Green synthesis of novel YMnO<sub>3</sub>-doped TiO<sub>2</sub> for enhanced visible-light- driven photocatalytic degradation of malachite green, *J. Environ. Manag.* 342 (2023), 118139.
- [33] I. Halomoan, Yoki Yulizar, Rizki Marcony Surya, Dewangga Oky Bagus Apriandau, Facile preparation of CuO-Gd<sub>2</sub>Ti<sub>2</sub>O<sub>7</sub> using Acmella uliginosa leaf extract for photocatalytic degradation of malachite green, *Mater. Res. Bull.* 150 (2022), 111726.
- [34] Yoki Yulizar, Dewangga Oky Bagus Apriandau, Rizki Marcony Surya, Fabrication of novel SnWO<sub>4</sub>/ZnO using Muntingia calabura L. leaf extract with enhanced photocatalytic methylene blue degradation under visible light irradiation, *Ceram. Int.* 48 (3) (2022) 3564–3577.
- [35] Adisty Maulida, Yoki Yulizar, Ridla Bakri, Dewangga Oky Bagus Apriandau, Rizki Marcony Surya, Synthesis and characterizations of Ce<sub>2</sub>Zr<sub>2</sub>O<sub>7</sub>-TiO<sub>2</sub> for increased photocatalytic activity toward degradation of methylene blue, *Ceram. Int.* 48 (19) (2022) 29523–29532.
- [36] Dewangga Oky Bagus Apriandau, Satoshi Nakayama, Kento Shibata, Fumiaki Amano, Ti-doped Fe<sub>2</sub>O<sub>3</sub> photoanodes on three-dimensional titanium microfiber felt substrate for photoelectrochemical oxygen evolution reaction, *Electrochim. Acta* 456 (2023), 142434.
- [37] L. Ye, Z. Cao, X. Liu, Z. Cui, Z. Li, Y. Liang, S. Zhu, S. Wu, Noble metal-based nanomaterials as antibacterial agents, *J. Alloys Compd.* 904 (2022), 164091.
- [38] S.J. Flora, V. Pachauri, Chelation in metal intoxication, *Int. J. Environ. Res. Publ. Health* 7 (7) (2010) 2745–2788.
- [39] J.S. Ajarem, S.N. Maodaa, A.A. Allam, et al., Benign Synthesis of Cobalt Oxide Nanoparticles Containing Red Algae Extract: Antioxidant, Antimicrobial, Anticancer, and Anticoagulant Activity, *J. Clust Sci.* 33 (2022) 717–728.
- [40] Nikolova, P. Maria, S. Chavali, Murthy, Metal Oxide Nanoparticles as Biomedical Materials, *Biomimetics* 5 (2) (2020) 27.
- [41] Jing Shen, Ziyi Liu, Henan Yu, Ye Jinshao, Long Yan, Pulin Zhou, He Baoyan, Systematic stress adaptation of *Bacillus subtilis* to tetracycline exposure, *Ecotoxicol. Environ. Saf.* 188 (2020), 109910.
- [42] J. Gajendiran, N. Sivakumar, C.P. Reddy, J.R. Ramya, The effect of calcination's temperature on the structural, morphological, optical behaviour, hemocompatibility and antibacterial activity of nanocrystalline Co<sub>3</sub>O<sub>4</sub> powders, *Ceram. Int.* 46 (4) (2020) 5469–5476.
- [43] C.T. Anuradha, Bio-inspired Senna auriculata flower extract assisted biogenic synthesis, characterization of cobalt oxide nanoparticles and their antibacterial and antifungal efficacy, *Ceram. Int.* 49 (7) (2023) 11689–11695.
- [44] C.A. Paul, E.R. Kumar, J. Suryakanth, A.F. Abd El-Rehim, Analysis and characterization of structural, morphological, thermal properties and colloidal stability of CuO nanoparticles for various natural fuels, *Ceram. Int.* 49 (19) (2023) 31193–31209.
- [45] C. Kumaran, I. Baskaran, K. Vanmathi Selvi, C. Senthamil Selvi, P. Rajkumar, S. Selvaraj, Antimicrobial activity of Cobalt doped Cerium Oxide (Co-CeO<sub>2</sub>) nanoparticles against selected food pathogens, *Int. Res. J. Multidiscip. Technovation* 5 (4) (2023) 27–36.